Synthesis, Structural, and Magnetic Characterization of a New Ferrimagnetic Oxide: $YFeMnO_5$

A. Muñoz,*,† J. A. Alonso,‡ M. J. Martínez-Lope,‡ and J. L. Martínez‡

Departamento de Física Aplicada, Escuela Politecnica Superior, Universidad Carlos III de Madrid, Avda. de la Universidad 30, E-28911 Leganés-Madrid, Spain, and Instituto de Ciencia de Materiales de Madrid, CSIC, Cantoblanco, E-28049 Madrid, Spain

Received May 14, 2004

A new ferrimagnetic oxide of stoichiometry $YFeMnO_5$ has been prepared in polycrystalline form by wet-chemistry procedures followed by thermal treatments under high oxygen pressure conditions. This material has been characterized by X-ray and neutron powder diffraction (NPD), magnetotransport, specific heat, and magnetization measurements. $YFeMnO_5$ is isostructural with RMn_2O_5 oxides; its crystal structure has been Rietveld refined from NPD data in the space group *Pbam*, and it contains infinite chains of $Mn^{4+}O_6$ octahedra sharing edges, linked together by $Fe^{3+}O_5$ pyramids and YO_8 units. A certain level of disorder has been found between both metallic positions; about 5% of Mn cations is replaced by Fe and vice versa. The magnetic measurements and the analysis of the temperature-dependent NPD patterns show that $YFeMnO_5$ orders below $T_c \approx 165$ K with a ferrimagnetic structure characterized by the propagation vector $\mathbf{k} = 0$. The spin arrangements for the Mn^{4+} ions (4f site) and Fe^{3+} ions (4h site) are given by the basis vectors $(0,0,F_z)$ and $(0,0,F_z')$, respectively. The Mn and Fe ordered magnetic moments are oriented along the *c* axis; at $T = 2.9$ K the magnitudes of the magnetic moments are 2.30(3) and −3.89(6) μ_B, respectively.

Introduction

The RMn_2O_5 compounds are among the few oxides showing a significant magnetoelectric effect,[1−5] implying a coupling between ferroelectricity and magnetic order in the system: the application of an external magnetic field leads to the appearance of an electrical polarization. This appealing property has recently impelled the study of this family of oxides which, in fact, were first described in the 1960s.[6,7] The orthorhombic crystal structure of the RMn_2O_5 compounds (space group *Pbam*) is attractive because it contains two crystallographic sites for Mn atoms, with different oxygen coordinations and oxidation states:[6−8] Mn^{4+} ions are located at the 4f sites, octahedrally coordinated to oxygens, whereas Mn^{3+} ions occupy the 4h sites and they are bonded by five oxygens, forming a distorted tetragonal pyramid. The structure contains infinite chains of edge-sharing $Mn^{4+}O_6$ octahedra, running along the *c* axis, and the different chains are interconnected by the $Mn^{3+}O_5$ pyramids and RO_8 scalenohedra.

The microscopic nature of the magnetic ordering in the RMn_2O_5 compounds has been studied by neutron diffraction. The first reports for R = Nd, Tb, Ho, Er, and Y[9,10] described an antiferromagnetic ordering at temperatures below 40 K. The magnetic structure is defined by the propagation vector $\mathbf{k} = (1/2,0,\tau)$, with τ depending on the type of R. The ordering for the Mn ions is helicoidal and the magnetic moments are placed in the *ab* plane. The rare-earth ions also become ordered at lower temperatures according to a sinusoidal magnetic structure. The magnetic structure was later revisited for R = Er and Tb,[11] and it seems that the amplitude of the moments for the Mn ions is also modulated. The magnetic structure of $DyMn_2O_5$ was analyzed in detail,[12] and it is given by two propagation vectors, $\mathbf{k}_1 = (1/2,0,0)$ and $\mathbf{k}_2 = (1/2,0,\tau)$. In the case of R = Eu, the magnetic structure is also defined by $\mathbf{k}_2 = (1/2,0,\tau)$, but τ varies with temperature and it blocks a commensurable value $\tau = 1/3$.[13] For $BiMn_2O_5$, the magnetic structure has also been studied in detail;[14−15] it is commensurable with the chemical cell, with a propagation vector $\mathbf{k} = (1/2,0,1/2)$.

* Corresponding author. E-mail: amunoz@fis.uc3m.es.
† Universidad Carlos III de Madrid.
‡ CSIC.

(1) Kadomtseva, A. M.; Popov, Y. F.; Vorobev, G. P.; Kamilov, K. I.; Makhov, P. N.; Tehranchi, M. M.; Phirouznia, A. *Physica B: Condensed Matter*, **2003**, 329−333, 856.
(2) Saito, K.; Kohn, K. *J. Phys.: Condens. Matter* **1995**, *7*, 2855.
(3) Inomata, A.; Kohn. *J. Phys.: Condens. Matter* **1996**, *8*, 2673.
(4) Popov, Y. F.; Kadomtseva, A. M.; Krotov, S. S.; Vorob'ev, G. P.; Lukina, M. M. *Ferroelectrics* **2002**, *279*, 147.
(5) Popov, Y. F.; Kadomtseva, A. M.; Krotov, S. S.; Vorob'ev, G. P.; Kamilov, K. I.; Lukina, M. M.; Tegranchi, M. M. *J. Exp. Theor. Phys.* **2003**, *96*, 961.
(6) Quezel-Ambrunaz, S.; Bertaut, E. F.; Buisson, G. *C. R. Acad. Sci.* **1964**, *258*, 3025.
(7) Bertaut, E. F.; Buisson, G.; Durif, A.; Mareschal, A.; Montmory, M. C.; Quezel-Ambrunaz, S. *Bull. Soc. Chim. Fr.* **1965**, 1132.
(8) Alonso, J. A.; Casais, M. T.; Martínez-Lope, M. J.; Martínez, J. L.; Fernández-Díaz, M. T. *J. Phys.: Condens. Matter* **1997**, *9*, 8515−8526.
(9) Buisson, G. *Phys. Status Solidi A* **1973**, *16*, 533.
(10) Buisson, G. *Phys. Status Solidi A* **1973**, *17*, 191.
(11) Gardner, P. P.; Wilkinson, C.; Forsyth, J. B.; Wanklyn, B. M. *J. Phys. C: Solid State Phys.* **1988**, *21*, 5653.
(12) Wilkinson, C.; Sinclair, F.; Gardner, P. P.; Forsyth, J. B.; Wanklyn, B. M. *J. Phys. C* **1981**, *14*, 1671.
(13) Polyakov, V.; Plakhty, V.; Bonnet, M.; Burlet, P.; Regnault, L. P.; Gavrilov, S.; Zobkalo, I.; Smirnov, O. *Physica B* **2001**, *297*, 208.
(14) Bertaut, E. F.; Buisson, G.; Quezel-Ambrunaz, S.; Quezel, G. *Solid State Commun.* **1967**, *5*, 25.
(15) Muñoz, A.; Alonso, J. A.; Casais, M. T.; Martínez-Lope, M. J.; Martínez, J. L.; Fernández-Díaz, M. T. *Phys. Rev. B* **2002**, *65*, 144423.

10.1021/cm049239v CCC: $27.50
Published on Web 09/14/2004

Aiming to induce new magnetic interactions in the members of the RMn_2O_5 family, we designed and prepared $YFeMnO_5$, obtained by replacing Mn^{3+} by Fe^{3+} in YMn_2O_5. It is the first reported member of a novel $RFeMnO_5$ (R = rare earths) series. This material has been characterized from the structural point of view from NPD data, which also allowed us to describe the low-temperature ferrimagnetic structure; these studies are complemented with macroscopic magnetic susceptibility and specific-heat measurements.

Experimental Section

$YMnFeO_5$ was prepared in polycrystalline form from citrate precursors obtained by a soft chemistry procedure. Stoichiometric amounts of analytical-grade Y_2O_3, $FeC_2O_4{\cdot}2H_2O$, and $MnCO_3$ were dissolved in citric acid; the solution was slowly evaporated, leading to an organic resin which was dried at 120 °C and slowly decomposed at temperatures up to 600 °C in air. High oxygen pressure treatments were performed in a Morris Research furnace, HPS-3210. About 2 g of the precursor powder was contained in a gold can during the oxygenation process. The sample was slowly heated to 900 °C at a final pressure of 200 bar and held at this temperature for 12 h. The product was finally cooled, under pressure, at 300 °C h^{-1} down to room temperature. Finally, the oxygen pressure was slowly released.

The dc susceptibility measurements were performed in a commercial SQUID magnetometer. They were obtained under a 1 kOe magnetic field in field-cooling conditions and for the temperature interval $1.8 < T < 800$ K. The ac susceptibility curves were measured under a small oscillating magnetic field of 0.3, 7, 33, and 321 Hz in the temperature range from $T =$ 2.8 K to $T = 285$ K. Different isothermal magnetization curves under magnetic fields ranging from −50 to 50 kOe and at $T =$ 1.8, 145, 180, 250, and 310 K have also been measured. The specific heat measurements were carried out in a semiadabatic calorimeter, using the heat-pulsed method for temperatures going from 1.9 to 273.9 K under a zero magnetic field.

Transport measurements were performed by the conventional four-probe technique in a pellet sintered under the synthesis conditions (900 °C under 200 bar O_2). Magnetotransport measurements were carried out under magnetic fields up to 9 T in a PPMS system from Quantum Design.

The neutron powder diffraction (NPD) patterns were acquired at the high-flux D20 diffractometer of the Institut Laue-Langevin in Grenoble (France). The sample, weighing 1 g, was packed in a vanadium holder of 6 mm diameter. The first pattern was collected at room temperature with a wavelength of 1.31 Å and a counting time of 1 h in the high-resolution mode. A set of NPD patterns was also dynamically collected in the temperature range $2.9 < T < 272.4$ K and with a wavelength of $\lambda = 2.433$ Å. The sample was first cooled at 2.9 K and then the temperature was ramped up at 2 K min^{-1} with a counting time of 5 min per diagram. The neutron diffraction patterns were analyzed with the Rietveld method,[16] using the FULLPROF program.[17] For the refinement of the profile, a pseudo-Voigt function was used to simulate the peak shape, and the background was fitted with a fifth-degree polynomial function. The coherent scattering lengths for Y, Fe, Mn, and O were 7.75, 9.45, −3.73, and 5.803 fm, respectively. In the final run the following parameters were refined: background coefficients, zero-point, half-width, pseudo-Voigt, and asymmetry parameters for the peak shape; scale factor, positional, thermal factors, and unit-cell parameters. The refinement of the low-temperature magnetic structure also included the magnitude of the magnetic moments at Fe and Mn positions.

Results

Preparation. $YFeMnO_5$ was obtained as a dark brown polycrystalline powder. The preparation of pure $YFeMnO_5$ oxide has been shown to be extremely favored by (i) the use of finely divided and homogeneous precursors and (ii) the final thermal treatment under high oxygen pressure. This material cannot be obtained from ceramic mixtures or by thermal treatments in air at ambient pressure: mixtures of the competitive $YMnO_3$ and $YFeO_3$ perovskites were always identified after all the thermal treatments in air at different temperatures. A single-phased $YFeMnO_5$ product could only be achieved by suitably annealing the precursor powders at 900 °C under 200 bar of O_2. This behavior can be easily understood since high oxygen pressure favors the full stabilization of the high oxidation state of manganese, Mn^{4+}. Figure 1 shows the XRD pattern of $YFeMnO_5$. It can be indexed in an orthorhombic unit-cell, isotypic to RMn_2O_5, with no additional peaks, which could indicate the presence of superstructures or departure of the mentioned symmetry.

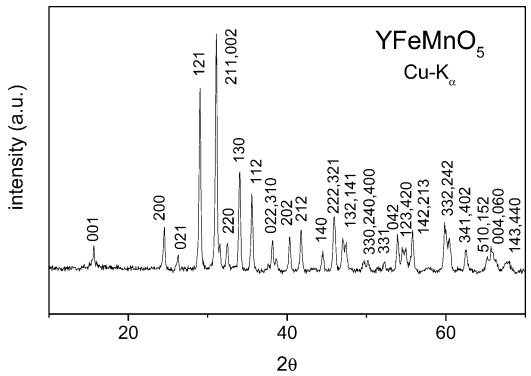

Figure 1. XRD pattern of $YFeMnO_5$, indexed in an orthorhombic unit cell with $a = 7.3121(7)$, $b = 8.5397(8)$, and $c =$ 5.7115(6) Å.

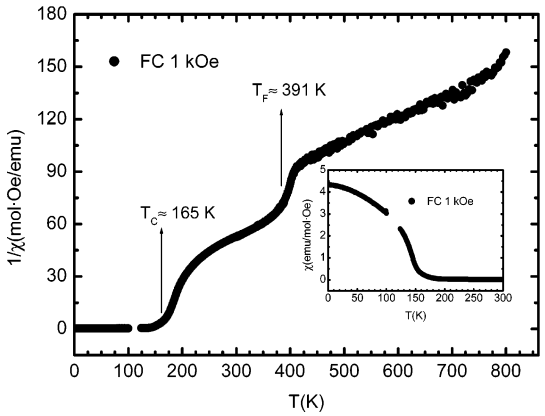

Figure 2. Thermal evolution of the inverse of the susceptibility measured under a 1 kOe magnetic field. Inset: Thermal evolution of the susceptibility below 300 K.

Magnetic Measurements. The thermal variation of the dc susceptibility is shown in Figure 2. As can be seen in the inset of Figure 2, the susceptibility undergoes a remarkable increase below 165 K, revealing the onset of a magnetic transition at $T_C \approx 165$ K. However, the inverse of the susceptibility does not present linear behavior immediately above T_C, and, furthermore, a second anomaly is observed at around $T_F \approx 391$ K. A linear Curie−Weiss fit in the high-temperature range 446−764 K gives a Weiss constant of $\theta_{Weiss} = -273(8)$ K, suggesting the presence of strong antiferromagnetic correlations, and an effective moment $\mu_{eff} = 7.60\ \mu_B$/f.u.,

(16) Rietveld, H. M. *J. Appl. Crystallogr.* **1969**, *2*, 65.
(17) Rodríguez-Carvajal, J. *Physica B* **1993**, *192*, 55.

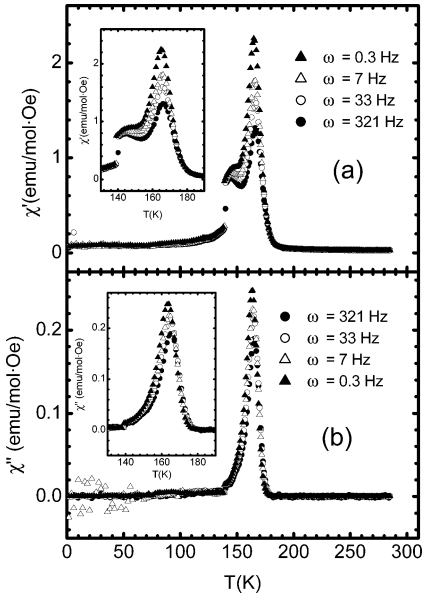

Figure 3. Temperature dependence of the ac susceptibility. The real part is reported in (a) and the imaginary in (b).

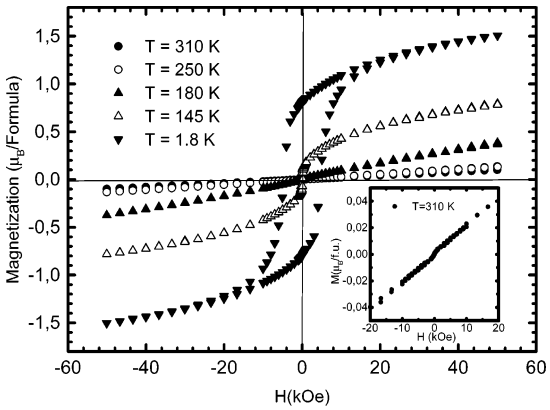

Figure 4. Isothermal magnetization curves.

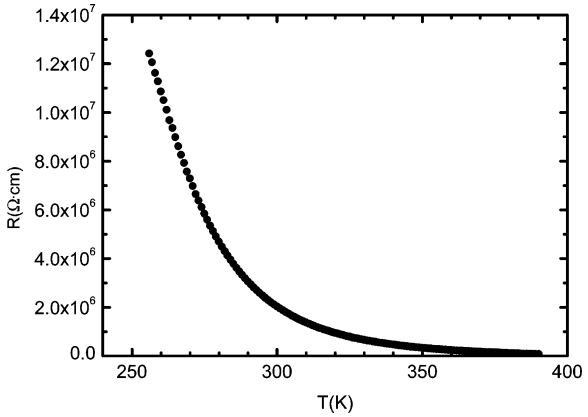

Figure 5. Thermal variation of the resistivity of $YFeMnO_5$.

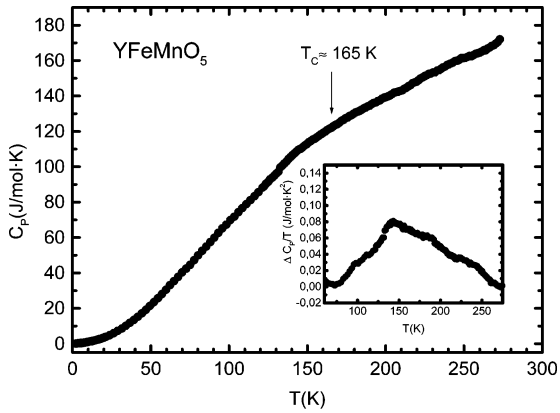

Figure 6. Thermal variation of the specific heat.

higher than that expected for high-spin Fe^{3+} ($t_{2g}^3e_g^2$) and Mn^{4+} (t_{2g}^3), of 7.07 μ_B/f.u. The thermal evolution of the ac susceptibility in the temperature range $1.8 < T < 285$ K is presented in Figure 3. On decreasing temperature, at around T_C, the in-phase χ' susceptibility shows a maximum, in good agreement with the magnetic transition observed in the dc susceptibility. This maximum in χ' presents a shoulder some 15 K below the maximum. Both anomalies are also observed in the out-of-phase χ'' susceptibility, although the low-temperature anomaly appears less clearly than in the χ' susceptibility. In the temperature range corresponding to the above-described shoulder, the ac susceptibility is frequency dependent. As the frequency increases, the temperature of the maximum undergoes a shift to higher values. In order to make clear the nature of the magnetic transitions, isothermal magnetization curves have also been measured. As can be seen in Figure 4, a hysteresis cycle is observed in the magnetization curves below $T_C \approx 165$ K, indicating the presence of a ferromagnetic component; in particular, at $T = 1.8$ K a remnant magnetization of 0.81 μ_B/formula is observed. The absence of saturation of the magnetic moments for the highest applied magnetic fields (5 T) is characteristic of ferrimagnetic materials or strongly canted ferromagnets. Above T_C, the magnetization curves apparently present a linear behavior, although a very small hysteresis is still observed, even at 310 K. This reveals the presence of a small ferromagnetic component. Microscopic neutron diffraction measurements described below demonstrate that the anomaly at $T_C = 165$ K indeed corresponds to the onset of a long-range ferrimagnetic structure. The presence of the high-temperature transition at $T_F \approx 391$ K will also be discussed later on, in light of the particular features of the crystal structure, showing some antisite disordering between Fe and Mn cations.

Transport Properties. The temperature dependence of the electrical resistivity is shown in Figure 5. A semiconducting behavior is observed in the temperature range 260−385 K. A considerably high resistivity of $\approx 2 \times 10^6$ Ω·cm is observed at RT; below 260 K the resistivity increases above 10^7 and overcomes the measuring range of our equipment. Ln ρ is linear with the reciprocal temperature, suggesting a thermally activated behavior; an Arrhenius fit gives an activation energy of 0.30 eV. The application of an external magnetic field up to 9 T did not show any significant change of resistivity, excluding the presence of magnetoresistance in the measured temperature range, well above T_C.

Specific Heat Measurements. The specific heat, measured in the temperature range $1.9 < T < 273.9$ K, is plotted as C_P versus T in Figure 6. The magnetic contribution is obtained by subtraction of the lattice contribution, simulated with three Einstein oscilators centered at 230, 500, and 850 K. The inset of Figure 6

Table 1. Structural Parameters after the Refinement of NPD Data of $YFeMnO_5$ at 295 K

atoms	positions	*x*	*y*	*z*	*B* (Å^2)	occupancy
Y	4g	0.1344(5)	0.1687(4)	0.00000	0.47(8)	1.0
Mn	4f	0.0000	0.5000	0.251(4)	0.52(9)	0.948(2)
Fe′	4f	0.0000	0.5000	0.251(4)	0.52(9)	0.052(2)
Fe	4h	0.3898(4)	0.3534(3)	0.50000	0.52(9)	0.948(2)
Mn′	4h	0.3898(4)	0.3534(3)	0.50000	0.52(9)	0.052(2)
O1	4e	0.0000	0.0000	0.260(2)	0.47(5)	1.0
O2	4g	0.1601(7)	0.4417(5)	0.00000	0.47(5)	1.0
O3	4h	0.1523(7)	0.4291(5)	0.50000	0.47(2)	1.0
O4	8i	0.3930(3)	0.2028(3)	0.2415(4)	0.47(5)	1.0
unit cell		a = 7.3121(7) Å	b = 8.5397(8) Å	c = 5.7115(6) Å	vol = 356.64(6) Å^3	
discrepancy factors		R_p = 4.9%	R_{wp} = 5.9%	R_{Bragg} = 3.1%	χ^2 = 2.4	

represents $\Delta C_p/T$ vs T, showing a distinct maximum at 141 K, with a shoulder at 170 K; both of them are identifiable with the peaks observed in the ac susceptibility, corresponding to the onset of magnetic ordering. The entropy variation in the magnetic transition can be evaluated through the expression $\Delta S = \int (C_{mag}/T)\, dT$; the entropy change in the temperature range $67.5 < T < 270$ K is 8.2 J·mol^{-1}·K^{-1}. The expected change for a set of free Fe^{3+} and Mn^4 ions is $\Delta S = R\ \mathrm{Ln}(2S_1 + 1) + R\ \mathrm{Ln}(2S_2 + 1) = 26.4$ J·mol^{-1}·K^{-1}, where $S_1 = {}^5/_2$ for Fe^{3+} and $S_2 = {}^3/_2$ for Mn^{4+}. Therefore, the experimental entropy change in the transition is around 31% of that expected.

At low temperature, in the $1.9 > T > 39.2$ K range, the best fit of the specific heat curve has been obtained by considering $C_P = \alpha T^3 + \beta T^{3/2}$; the cubic term comes from the lattice contribution to the specific heat and the second term corresponds to the magnetic excitations with ferromagnetic character. The linear term that should appear in the specific heat expression, which is associated with the free electrons, was negligible, in good agreement with the insulating features of the compound. The fit has given $\alpha = 0.11(1)$ mJ/mol·K^4 and $\beta = 28.3(1)$ mJ/mol·K$^{5/2}$. On considering that the Debye temperature, Θ_D, is related to α through the expression $\Theta_D = (12\pi^4 nR/5\alpha)^{1/3}$, n being the number of atoms per formula unit and R the gas constant, the Debye temperature is $\Theta_D = 520(20)$ K.

Neutron Diffraction: Crystallographic Structure. The crystallographic structure has been refined from a NPD pattern acquired at room temperature (RT) with a wavelength $\lambda = 1.31$ Å. The pattern was fitted in the orthorhombic space group *Pbam*, with unit-cell parameters $a = 7.3121(7)$ Å, $b = 8.5397(8)$ Å, and $c = 5.7115(6)$ Å. The crystal structure of $NdMn_2O_5$ was used as a starting model.[18,19] Y atoms were located at 4g (x,y,0) positions, Mn at 4f (0,${}^1/_2$,z) sites, Fe at 4h (x,y, ${}^1/_2$), and the four crystallographically independent oxygen atoms at 4e (0,0,z), 4g, 4h, and 8i (x,y,z) positions. The good agreement between the calculated and observed patterns after the Rietveld refinement is displayed in Figure 7. The main structural parameters obtained in the fit are presented in Table 1. The presence of a certain level of anti-site disorder between Fe and Mn cations was checked; a 5.2% of Mn positions at 4f sites are occupied by Fe cations (probably Fe^{4+}) and vice versa, as shown in Table 1. A selection of the most important atomic distances and angles is listed in Table 2.

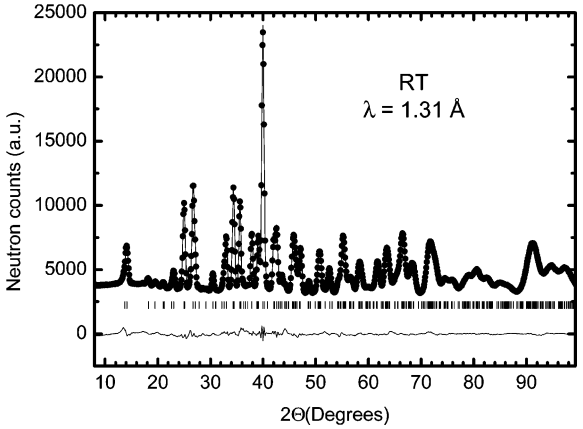

Figure 7. Observed (solid circles), calculated (solid line), and difference (bottom line) NPD patterns for room temperature. The row of tic marks corresponds to the Bragg reflections of $YFeMnO_5$.

Table 2. Selected Interatomic Distances (Å) and Angles (deg) of $YFeMnO_5$ at 295 K

$Mn^{4+}O_6$		$Y^{3+}O_8$	
Mn−O2 (×2)	1.916(18)	Y−O1 (×2)	2.290(7)
Mn−O3 (×2)	1.906(18)	Y−O2	2.339(5)
Mn−O4 (×2)	1.901(3)	Y−O2	2.452(6)
⟨Mn−O⟩	1.908(13)	Y−O4 (×2)	2.358(4)
$Fe^{3+}O_5$		Y−O4 (×2)	2.494(4)
Fe−O1 (×2)	2.024(7)	⟨Y−O⟩	2.384(5)
Fe−O3	1.854(6)		
Fe−O4 (×2)	1.958(3)	Mn−Mn	2.86(3)
⟨Fe−O⟩	1.964(5)	Mn−Mn	2.85(3)
		Fe−Fe	2.978(4)
Fe−O1−Fe	94.5(4)		
Mn−O2−Mn	94.3(14)	Mn−O3−Mn	99.0(14)
Mn−O3−Fe	129.9(7)	Mn−O4−Fe	127.2(5)

A view of the crystallographic structure along the c axis is displayed in Figure 8. There are two different oxygen environments for the atoms that occupy the 4f and 4h sites. At the 4f site, the Mn^{4+} ions are inside the $Mn^{4+}O_6$ distorted octahedra, whereas at the 4h site, the Fe^{3+} ions form $Fe^{3+}O_5$ distorted tetragonal pyramids. The pyramids share edges to form dimer units Fe_2O_{10}, linked via O1 oxygens. The structure contains infinite chains of $Mn^{4+}O_6$ octahedra sharing edges via O2 and O3 oxygens, running along the c axis. The different chains of $Mn^{4+}O_6$ are interconnected through the Fe_2O_{10} pyramidal dimer units via O3 and O4 oxygens.

Neutron Diffraction: Magnetic Structure Resolution. The magnetic structure was analyzed from the NPD patterns collected in the temperature range $2.9 <$

(18) Euzen, P.; Leone, P.; Gueho, C.; Palvadeau, P. *Acta Crystallogr. C* **1993**, *49*, 1875.
(19) Alonso, J. A.; Casais, M. T.; Martínez-Lope, M. J.; Rasines, I. *J. Solid State Chem.* **1997**, *129*, 105−112.

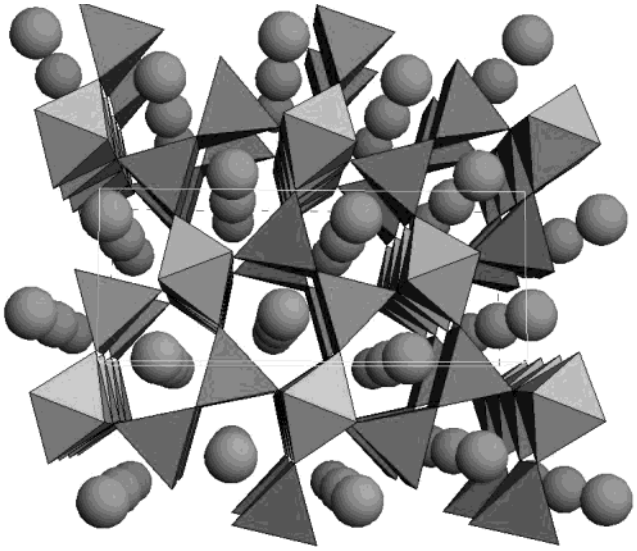

Figure 8. View of the crystallographic structure of $YFeMnO_5$, approximately along the *c* axis. Octahedra and tetragonal pyramids correspond to $Mn^{4+}O_6$ and $Fe^{3+}O_5$ polyhedra. Octahedra share edges, forming infinite chains along the *c* axis. Pyramids form dimer units, linking together the chains of octahedra. Spheres represent the Y atoms.

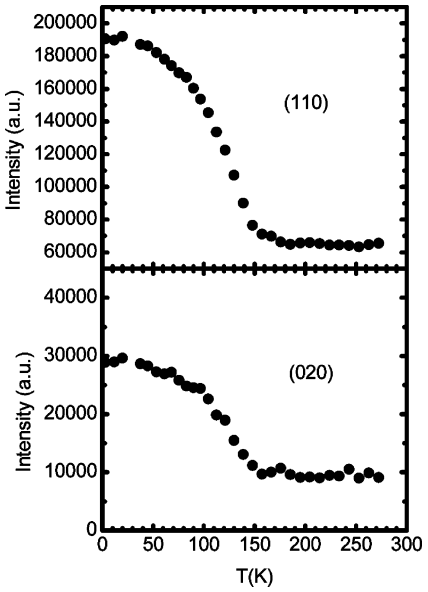

Figure 9. Thermal evolution of the intensity of the (110) and (020) reflections.

$T < 272.4$ K with $\lambda = 2.433$ Å. From the NPD pattern measured at 166.5 K and below, the intensities of some Bragg reflections (for instance, (110) and (020)) start to increase as the temperature decreases (see Figure 9). This observation confirms the onset of a long-range magnetic ordering, in agreement with the susceptibility and specific heat measurements. The monotonic increase of the intensity of these low-angle reflections, to reach saturation at low temperature, indicates that the magnetic structure remains stable down to 2.9 K. Let us point out that no extra magnetic reflections appear out of the Bragg positions allowed by the *Pbam* space group. Therefore, the magnetic structure is defined by the propagation vector $\mathbf{k} = 0$.

For the resolution of the magnetic structure, we have considered those solutions that are compatible with the crystal symmetry of $YFeMnO_5$, which have been obtained by following the representation analysis technique described by Bertaut.[20] For $\mathbf{k} = 0$, the small group $G_\mathbf{k}$ coincides with the *Pbam* space group and, according to the Kovalev's Tables,[21] its eight irreducible representations are those shown in Table 3. The notation for the Mn atoms in the 4f site (Mn1) is 1 ($0,{}^1/_2,z$), 2 ($^1/_2,0,-z$), 3 ($0,{}^1/_2,-z$), and 4 ($^1/_2,0,z$). The Fe atoms in the 4h site (Fe2) are denoted as 5 ($x,y,{}^1/_2$), 6 ($-x,-y,{}^1/_2$), 7 ($-x + {}^1/_2,y + {}^1/_2,{}^1/_2$) and 8 ($x + {}^1/_2,-y + {}^1/_2,{}^1/2$). The possible solutions for each one of the irreducible representations are given in Table 4.

Table 3. Irreducible Representations of the $G_\mathbf{K} = Pnma$ for k = 0; τ Is the Translation ($^1/_2,^1/_2,0$)

	1	$2_x/(\tau)$	$2_y/(\tau)$	2_z	$\bar{1}$	$\bar{1}2_x/(\tau)$	$\bar{1}2_y/(\tau)$	$\bar{1}2_z$
Γ^1	1	1	1	1	1	1	1	1
Γ^2	1	1	1	1	−1	−1	−1	−1
Γ^3	1	1	−1	−1	1	1	−1	−1
Γ^4	1	1	−1	−1	−1	−1	1	1
Γ^5	1	−1	1	−1	1	−1	1	−1
Γ^6	1	−1	1	−1	−1	1	−1	1
Γ^7	1	−1	−1	1	1	−1	−1	1
Γ^8	1	−1	−1	1	−1	1	1	−1

After checking the different solutions, the magnetic spins arrangement that gives a better agreement with the experimental data corresponds to the $(0,0,F_z)$ and $(0,0,F_z')$ basis vectors of the 4f and 4h sites, respectively. Regarding the magnetic contribution to the Bragg reflections, it has been considered that the 4f and 4h sites are only occupied by the Mn and Fe atoms, respectively. The F_z and F_z' basis vectors imply that the relationships among the magnetic moments is $m_{1z} = m_{2z} = m_{3z} = m_{4z}$ for the Mn atoms and $m_{5z} = m_{6z} = m_{7z} = m_{8z}$ for the Fe atoms. All the magnetic moments are collinear and lie along the *z*-axis; the coupling between magnetic moments within the Mn magnetic sublattice is ferromagnetic, and a similar coupling also exists for the Fe atoms. As shown in Table 5, the refined magnetic moments are 2.30(3) μ_B for the Mn atoms and −3.89(6) μ_B for the Fe atoms at $T = 2.9$ K. The opposite sign of the magnetic moments implies that the coupling Mn and Fe spins is antiferromagnetic; therefore, the global magnetic structure is ferrimagnetic. These values are somewhat reduced with respect to those expected for Mn cations in the 4f site (Mn^{4+}, electronic configuration $t_{2g}{}^3e_g{}^0$, expected moment of 3 μ_B) and for Fe cations in the 4h site (Fe^{3+}, electronic configuration $t_{2g}{}^3e_g{}^2$, expected moment of 5 μ_B), which can be originated by covalency effects. Figure 10 illustrates the good agreement between the experimental NPD pattern and the calculated one at $T = 2.9$ K, including the considered ferrimagnetic structure. A schematic view of the magnetic structure is shown in Figure 11. The thermal evolution of the ordered magnetic moments for both Mn^{4+} and Fe^{3+} ions is displayed in Figure 12.

Discussion

$YFeMnO_5$ derives from the parent YMn_2O_5 oxide (containing one Mn^{3+} and one Mn^{4+} cation per formula)

(20) Bertaut, E. F. *Magnetism*; Rado, G. T., Shul, H., Eds. Academic: New York, 1963; Vol. III, Chapter 4.
(21) Kovalev, O. K. *Representation of the Crystallographic Space Group*, 2nd ed.; Stokes, H. T., Hatch, D. M., Eds.; Gordon and Breach: New York, 1993.

Table 4. Basis Vector for the 4h and 4f Sites

	Mn(4f)	Fe(4h)
Γ^1	$(0,0,G_z)$	$(0,0,C_z')$
Γ^2	$(0,0,A_z)$	$(A_x',G_y',0)$
Γ^3	$(F_x,G_y,0)$	$(F_x',C_y',0)$
Γ^4	$(C_x,A_y,0)$	$(0,0,G_z')$
Γ^5	$(G_x,F_y,0)$	$(C_x',F_y',0)$
Γ^6	$(A_x,C_y,0)$	$(0,0,A_z')$
Γ^7	$(0,0,F_z)$	$(0,0,F_z')$
Γ^8	$(0,0,C_z)$	$(G_x',A_y',0)$

$\mathbf{F} = \mathbf{m}_1 + \mathbf{m}_2 + \mathbf{m}_3 + \mathbf{m}_4$; $\mathbf{F}' = \mathbf{m}_5 + \mathbf{m}_6 + \mathbf{m}_7 + \mathbf{m}_8$; $\mathbf{G} = \mathbf{m}_1 - \mathbf{m}_2 + \mathbf{m}_3 - \mathbf{m}_4$; $\mathbf{G}' = \mathbf{m}_5 - \mathbf{m}_6 + \mathbf{m}_7 - \mathbf{m}_8$
$\mathbf{C} = \mathbf{m}_1 + \mathbf{m}_2 - \mathbf{m}_3 - \mathbf{m}_4$; $\mathbf{C}' = \mathbf{m}_5 + \mathbf{m}_6 - \mathbf{m}_7 - \mathbf{m}_8$; $\mathbf{A} = \mathbf{m}_1 - \mathbf{m}_2 - \mathbf{m}_3 + \mathbf{m}_4$; $\mathbf{A}' = \mathbf{m}_5 - \mathbf{m}_6 - \mathbf{m}_7 + \mathbf{m}_8$

Table 5. Results from the Magnetic Structure Determination from NPD Data at $T = 2.9$ K

	Mn(4f)	Fe(4h)
solution	$(0,0,F_z)$	$(0,0,F_z')$
values (μ_B)	(0,0,2.30(3))	(0,0,−3.89(6))
$\lvert\mathbf{m}\rvert$ (μ_B)	2.30(3)	3.89(6)
discrep. factors	R_B(nuclear) = 3.6%; R_B(magn.) = 5.8%; $\chi^2 = 1.9$	

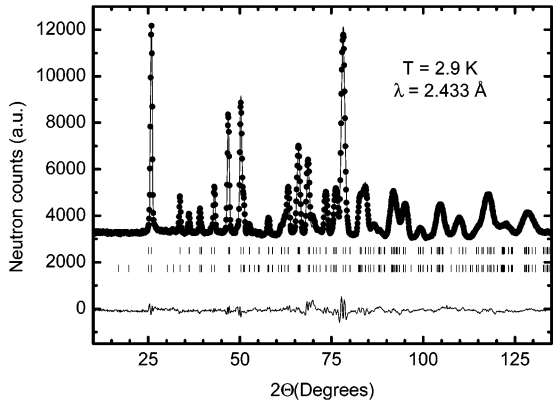

Figure 10. Observed (solid circles), calculated (solid line), and difference (bottom line) NPD patterns for $T = 2.9$ K. The first row of tic marks correspond to the Bragg reflections of $YFeMnO_5$ and the second row to the magnetic peaks.

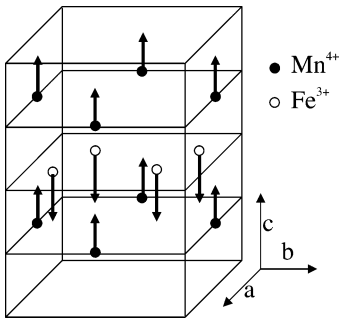

Figure 11. A schematic view of the magnetic structure. For sake of clarity only the magnetic atoms are represented.

by full replacement of Mn^{3+} by Fe^{3+} cations. The crystal structure of $YFeMnO_5$, refined from NPD data is tightly related to that of RMn_2O_5 oxides, as expected from the similarity in ionic radii between Fe^{3+} and Mn^{3+}, of 0.645 Å in 6-fold coordination and high-spin state for both cations.[22] Since no structural details on the parent YMn_2O_5 have been reported, a comparison can be established with the crystal structure of $HoMn_2O_5$,[8] given the similarity in ionic sizes of the Y^{3+} cation (1.019 Å) and Ho^{3+} (1.015 Å) in 8-fold coordination.[22] In $HoMn_2O_5$ (and other RMn_2O_5 compounds), the $Mn^{4+}O_6$ octahedra are fairly flattened,[8,18] with two bonds significantly shorter than the remaining four bonds (e.g., Mn1−O3 of 1.836(8) Å for the Ho compound); the average Mn−O distance is 1.902 Å. In contrast, in $YFeMnO_5$ the $Mn^{4+}O_6$ octahedra are much less distorted, exhibiting very similar Mn−O bonds distances with an average value of 1.91 Å. Regarding the tetragonal pyramids, $Fe^{3+}O_5$ units are flattened, as the axial Fe−O3 bond length is the shortest one, which is in contrast to that observed in $HoMn_2O_5$, where the Mn2−O3 bond in the axial position is the longest one in the $Mn^{3+}O_5$ pyramids. Additionally, the equatorial Fe−O1 and Fe−O4 bond distances (forming the square basis of the pyramid) are longer in $Fe^{3+}O_5$ than the corresponding Mn−O distances in the $Mn^{3+}O_5$ units of the RMn_2O_5 compounds. This is probably related to the Jahn−Teller character of Mn^{3+} cations, favoring an increase of the axial bond lengths in the $Mn^{3+}O_5$ pyramids, in contrast with the non-Jahn−Teller character of Fe^{3+} ($3d^5$ configuration). With respect to the oxygen coordination of Y^{3+} cations, it can be described as $Y^{3+}O_8$ bicapped prisms, with average ⟨Y−O⟩ distances of 2.384 Å, in good agreement with the ⟨Ho−O⟩ bond lengths of 2.381 Å observed in $HoMn_2O_5$.

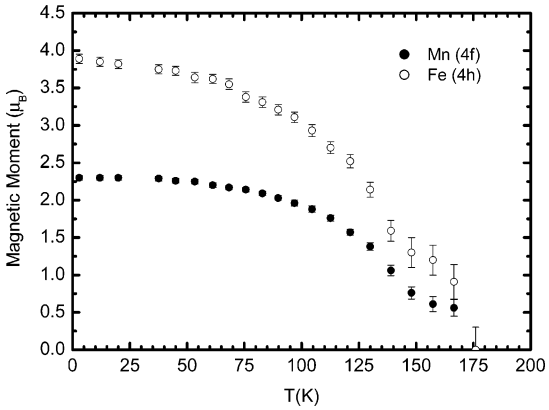

Figure 12. Thermal evolution of the module of the magnetic moments for the Mn^{4+} and Fe^{3+} ions.

$YFeMnO_5$ is a new ferrimagnetic material, with a magnetic ordering temperature of $T_C \approx 165$ K, as shown from the macroscopic magnetic measurements and confirmed by the microscopic neutron diffraction data. In $YFeMnO_5$, the Mn and Fe magnetic moments, at the 4f and 4h crystallographic sites of the *Pbam* space group, respectively, lie along the *z* direction and are antiferromagnetically coupled, giving rise to a global ferrimagnetic structure.

The comparison of the magnetic ordering of $YFeMnO_5$ with that observed in the RMn_2O_5 (R = rare earths and Y, Bi) isostructural compounds shows some important differences that must be highlighted. First, the ordering

(22) Shannon, R. D. *Acta Crystallogr.* **1976**, *A32*, 751.

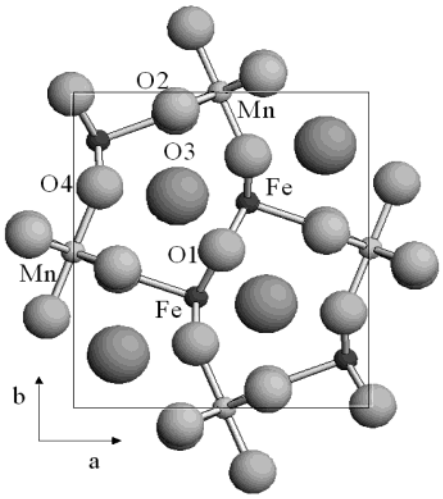

Figure 13. Top view of the crystal structure of $YFeMnO_5$, along the *c* axis, displaying the superexchange paths for magnetic coupling via O1 for the Fe^{3+} dimer units and via O3 and O4 between Fe^{3+} and Mn^{3+}. Large spheres represent Y.

in the RMn_2O_5 compounds appears at around 40 K, whereas $YFeMnO_5$ orders at a much higher temperature, $T_C \approx 165$ K. Second, in most of the RMn_2O_5 compounds the magnetic structure is incommensurate, with $\mathbf{k} = (^1/_2,0,\tau)$; however, in $YFeMnO_5$ the magnetic structure is commensurate, with $\mathbf{k} = 0$. Besides, in the RMn_2O_5 compounds, the magnetic moments lie on the *ab* planes, whereas in $YFeMnO_5$ the magnetic moments for both Mn and Fe atoms are oriented along the *c* direction. The presence of Fe^{3+} cations is not only responsible for the different strengths of the magnetic coupling but also for the signs of some of the superexchange interactions.

A comparison between the Néel antiferromagnetic-ordering temperatures for the isostructural $YMnO_3$ and $YFeO_3$ perovskites, of $T_N \approx 42$ K and $T_N \approx 650$ K, respectively,[23−25] already gives an idea of the much stronger superexchange interactions expected between the Fe magnetic moments. In $YFeMnO_5$ we could expect an even higher long-range ordering temperature if the FeO_5 pyramidal units were all connected through common oxygens; in fact, the FeO_5 pyramids form dimer units via O1 oxygens, which are interconnected through the $[MnO_6]_\infty$ chains, as observed in Figures 8 and 13. It seems reasonable to think that the strong superexchange Fe−O1−Fe interactions within the dimer Fe_2O_{10} units trigger the onset of the magnetic ordering of the Fe^{3+} spins well above T_C. Given the Fe−O1−Fe angles close to 90° within the dimers (Table 2), these interactions are ferromagnetic in origin, according to the Goodenough−Kanamori rules.[26,27] It is difficult to assign a temperature for the onset of ferromagnetic coupling of the Fe^{3+} pairs at the dimer units. The fact that the specific heat curve (Figure 6) shows a broad peak with an associated entropy much smaller than that corresponding to the full magnetic ordering of the complete set of magnetic moments in the structure suggests that an important fraction of the magnetic couplings have been satisfied at higher temperatures, above 300 K. The anomaly at $T_F = 391$ K could be related to the establishment of the short-range coupling within the dimer units. However, this hypothesis seems not to be supported by the fact that the Curie−Weiss fit above 446 K yields a strongly negative Weiss temperature of −273(8) K, indicating the presence of predominant antiferromagnetic interactions in the 446−764 K range and suggesting that the ferromagnetic coupling between Fe^{3+} pairs is already (at least partially) established in this high-temperature range. The large paramagnetic moment of 7.60 μ_B/f.u. also supports the presence of ferromagnetically coupled Fe^{3+}-spin dimers in this temperature range.

The establishment of a long-range magnetic ordering across the solid plays at temperatures close to T_C. This happens via a double mechanism: (i) through Mn−O−Fe−O−Mn paths, connecting adjacent chains (see Figure 13), and (ii) along the $[MnO_6]_\infty$ chains, involving Mn^{4+}−(O2,O3)−Mn^{4+} interactions that lead to the long-range magnetic ordering of Mn^{4+} spins. The superexchange interactions Fe^{3+}−(O3,O4)−Mn^{4+} are antiferromagnetic in origin, whereas the Mn^{4+}−O−Mn^{4+} interactions have, in this case, a positive sign, although they can be negative as it happens in RMn_2O_5 oxides, discussed below. This double mechanism for the establishment of the long-range magnetic ordering accounts for the double peak observed in the ac susceptibility curve. Concerning the evolution of the NPD patterns, the observed inflection in the variation of the ordered Fe and Mn magnetic moments (Figure 12) could be a reminiscence of the mentioned double mechanism.

It is interesting to carefully examine the magnetic interactions happening along the chains of Mn^{4+} ions (Mn at 4f site). They are arranged in (001) planes, located at the $z = z_0$, $z = 1 - z_0$, and $z = -z_0$ planes ($z_0 = 0.251(4)$). There is an interleaved plane of Y^{3+} ions ($z = 0$) between the $z = z_0$ and $z = -z_0$ planes and a plane of Fe^{3+} ions ($z = ^1/_2$) intercalated between the $z = z_0$ and $z = 1 - z_0$ planes. The distances between the Mn^{4+} ions belonging to different (001) planes are $2z_0$ for those placed at the $z = z_0$ and $z = -z_0$ planes and $1 - 2z_0$ for those placed at the $z = z_0$ and $z = 1 - z_0$. We define the interplane superexchange interaction J_1, between the Mn^{4+} ions of the $z = z_0$ and $z = -z_0$ planes (Mn−O2−Mn), and J_2, associated with the direct exchange interactions between the $z = z_0$ and $z = 1 - z_0$ planes (Mn−O3−Mn); besides, J_3, the indirect superexchange interactions between the $z = z_0$ and $z = 1 - z_0$ planes through the Fe^{3+} ions (or Mn^{3+} ions for the RMn_2O_5 compounds), must be included. The values of the exchange interactions parameters depend on the bonding distances and angles. For z_0 different from 0.25, the distances $1 - 2z_0$ and $2z_0$ are different, and J_1 and J_2 have different values and different signs. In general, J_3 is a second-order term and its importance depends on its relative value with respect to J_2. For most of the RMn_2O_5 oxides $z_0 > 0.25$, so J_1 and J_2 would have different signs and their values should follow the relationship $|J_1| < 4|J_2|$,[9] giving rise to a magnetic structure with an incommensurate k_z value. In YFe-

(23) Muñoz, A.; Alonso, J. A.; Casais, M. T.; Martínez-Lope, M. J.; Martínez, J. L.; Fernández-Díaz, M. T. *J. Phys.: Condens. Matter* **2002**, *14*, 3285−3294.
(24) Georgiev, D. G.; Krezhov, K. A.; Nietz, V. V. *Solid State Commun.* **1995**, *96*, 535.
(25) Nereson, N.; Arnold, G. *J. Chem. Phys.* **1970**, *53*, 2818.
(26) Goodenough, J. B. *Phys. Rev.* **1955**, *100*, 564.
(27) Kanamori, J. *J. Phys. Chem. Solids* **1959**, *10*, 87.

MnO_5, z_0 is very close to 0.25 and both distances are very similar, 2.85(3) and 2.86(3) Å; therefore, J_1 and J_2 must be similar and have the same sign, which would explain $k_z = 0$ and a ferromagnetic coupling of Mn^{4+} spins along the chains.

The presence of a small remanent magnetization from T_C up to 310 K and the second transition in the dc susceptibility at around $T_F \approx 391$ K are intriguing, if we admit that the Fe dimers are already coupled above this temperature. Of course, the small magnitude of the involved magnetic moments makes it impossible to analyze this effect by NPD, at temperatures above T_C. Furthermore, we exclude the presence of possible impurities (undetected by diffraction methods) such as $YMnO_3$ and $YFeO_3$ perovskites as responsible for this anomaly since these oxides become antiferromagnetically ordered at $T_N \approx 42$ K and $T_N \approx 650$ K, respectively; this latter compound does not show magnetic singularities around 391 K. Ferromagnetic phases such as Fe, Fe_3O_4, or Mn_3O_4 are not stable under the highly oxidizing synthesis conditions. We propose that the mentioned phenomenon at $T_F \approx 391$ K is a consequence of the significant anti-site disordering observed between Mn and Fe sublattices in $YFeMnO_5$, of about 5%. This disorder implies the occurrence of Fe^{4+} cations at the octahedral 4f positions of the crystal structure, thus providing $Fe^{4+}-O-Fe^{3+}$ superexchange paths between the FeO_6 octahedra and the FeO_5 pyramids, characterized by a strong superexchange coupling strength. In other words, we could consider the presence of scattered clusters of YFe_2O_5 with an ordering temperature of $T_F \approx 391$ K (ferrimagnetic o ferromagnetic), with which the remnant magnetization found above T_c is plausible to be associated. Pure YFe_2O_5 oxide has not been reported to date since its preparation would require the use of very high O_2 pressures to stabilize 100% Fe^{4+} at the octahedral positions of the crystal structure. The isolation of intermediate materials belonging to the solid solution $YFe_{1+x}Mn_{1-x}O_5$, with enhanced T_C's, is in progress.

Conclusions

We describe a new ferrimagnetic oxide obtained by replacing Mn^{3+} by Fe^{3+} in the parent YMn_2O_5 compound. The crystal structure of $YFeMnO_5$ is isotypic with that of RMn_2O_5 materials (space group *Pbam*) and contains chains of edge-linked $Mn^{4+}O_6$ octahedra connected via dimer groups of square pyramids $Fe^{3+}O_5$. A feature of the Fe compound is that the square pyramids are flattened, showing shorter axial distances with respect to the $Mn^{3+}O_5$ pyramids in RMn_2O_5. $YFeMnO_5$ is semiconducting with a large room-temperature resistivity; the magnetic susceptibility and the thermal evolution of the NPD patterns reveal the onset of a ferrimagnetic structure below $T_c \approx 165$ K, characterized by the propagation vector $\mathbf{k} = 0$. The magnetic sublattices of Mn^{4+} ions, at 4f sites, and Fe^{3+} ions, at 4h sites, are antiferromagnetically coupled, giving rise to a net ferrimagnetic structure; for both cations the magnetic moments are orientated along the *c* direction. At $T = 2.9$ K the values of the ordered magnetic moments are 2.30(3) and $-3.89(6)$ μ_B for the Mn and Fe atoms, respectively. The refinement of the NPD patterns reveals the presence of a certain anti-site disorder in the sample, with 5% of Mn atoms located at Fe positions, and vice versa. It is not disregarded that this disorder implies the presence of clusters of YFe_2O_5 oxide, where strong magnetic interactions are thought to be promoted via $Fe-O-Fe$ superexchange paths; the presence of these clusters accounts for the anomaly observed in the magnetic susceptibility above room temperature.

Acknowledgment. We thank the financial support of CICyT to the Projects MAT2001-0539 and MAT2002-1329, and we are grateful to ILL for making all facilities available.

CM049239V